Progress in Natural Science: Materials International 26 (2016) 197–203

HOSTED BY

ELSEVIER

Contents lists available at ScienceDirect

Progress in Natural Science: Materials International

journal homepage: www.elsevier.com/locate/pnsmi

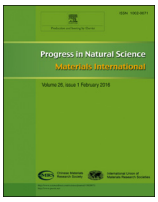

Original Research

Fatigue crack propagation behavior of Ni-based superalloys after overloading at elevated temperatures

Xinyue Huang [a,*], Liang Wang [a], Yunming Hu [b], Guangping Guo [a], David Salmon [b], Ying Li [a], Wenxia Zhao [c]

[a] National Key Laboratory of Science and Technology on Advanced High Temperature Structural Materials, Beijing Institute of Aeronautical Materials, Beijing 100095, China

[b] MTS Systems Corporation, Eden Prairie, MN 55344, USA

[c] Beijing Key Laboratory of Aeronautical Materials Testing and Evaluation, Beijing Institute of Aeronautical Materials, Beijing 100095, China

ARTICLE INFO

Article history:
Received 22 December 2015
Accepted 17 February 2016
Available online 20 April 2016

Keywords:
High temperature fatigue
Fatigue crack propagation rate
Overloading
Crack closure
Superalloys

ABSTRACT

The fatigue crack propagation behavior of three superalloys subjected to a single overloading at elevated temperatures was investigated. The fatigue crack propagation rate FCPR versus stress intensity factor range data $da/dN-\Delta K$ were calculated using the two-point secant method. It was found that the crack growth rates of the investigated materials were retarded after overloading with an overload ratio $R_{OL}=1.6$. The size of the plastic zone in the front of the crack tip and its relation to loading level were discussed. The overload retardation effects are attributed to crack closure. The fatigue damage in the plastic zone can also be a factor to explain the overload retardation.

1. Introduction

A major use of nickel-based superalloys is to manufacture aeroengine components, such as turbine disks, vanes and blades, subjected to high stress in high temperature environments. The structural integrity specifications for aeroengines require that a damage tolerant design philosophy should be applied to the critical components. Experimental fatigue crack propagation rate (FCPR) data for superalloys are fundamental in order to characterize material fatigue and fracture behavior in the presence of discontinuities or defects. The standard experiments for studying crack propagation behavior are the test methods to produce an empirical relationship between FCPR data da/dN (a is the crack length and N the loading cycles) and driving force, characterized by stress intensity factor K, such as ΔK, K_{max} etc.

In general, FCPR is mainly a function of driving force, but there are also some additional influencing factors. For the $da/dN - \Delta K$ data of aeroengine materials working at elevated temperatures, the main factors influencing material response are stress ratio $R=\sigma_{min}/\sigma_{max}$, frequency of fatigue cycling f, and testing temperature T [1]. These factors can be function either individually or combined, and are of particular interests. According to the researches on fatigue crack behavior for a variety of superalloys, including IN 718 and Waspaloy [2], Haynes 230 [3], and IN-100 [4], it is found that the FCPR is affected significantly by testing temperature for the stress ratio $R=0.1$. The FCPRs is faster when temperature is higher for these materials. The effect of stress ratio R on FCPR shows a monotonic trend, with higher R values leading to faster FCPRs [5–7].

In addition, the loading sequences are a more important factor to affect FCPR. This effect has been well studied for many aluminum alloys, steels and titanium alloys, which are widely used for airframes. As summarized by Schijve [8] the proposed mechanisms to explain the retardation effect of overloading are associated with several aspects, including the residual compression stress in the plastic zone ahead of the crack tip, as well as the plasticity induced crack closure caused by residual plastic deformation in the crack wake. Some other mechanisms are proposed recently, such as the strain hardening in the plastic zone at the crack tip [9] and the crack blunting during overloads [10]. But the available models are mostly used for the prediction of fatigue behavior at room temperature. The loading sequence effect is a more complex one and it is a combination or superposition factor which covers the others factors mentioned above. Although only limited papers are available for superalloys, it was found that some superalloys, e.g. IN-100 [4] at room and elevated temperatures, IN 718 at 400 °C [11] and 650 °C [12], Waspaloy [13] at room temperature, and Hastelloy C2000 [10], show similar overload retardation effects.

* Corresponding author.
E-mail address: beihehuang@sins.com (X. Huang).

Peer review under responsibility of Chinese Materials Research Society.

http://dx.doi.org/10.1016/j.pnsc.2016.03.007

There is still a lack of understanding about the mechanism of FCPR retardation after overloading for superalloys at elevated temperatures. In this paper the effect of single overload on FCPR at constant stress amplitude is investigated for three superalloys at elevated temperatures by fatigue tests and SEM fractography. The possible mechanisms of the overload retardation effect are discussed.

2. Materials and experimental

Three kinds of nickel base superalloys were chosen in the present investigation: a wrought alloy GH4169 (Alloy A) with the nominal composition of (0.015–0.08)C–17.0Cr–(0.015–0.08)Mo–(4.75–5.50)(Nb+Ta)–15.0Fe–(0.3–0.7)Al–(0.75–1.15)Ti–Ni Balance, a powder metallurgy (PM) alloy (Alloy B) with the nominal composition of 4.45Al–1.87Ti–9.20Cr–4.51Mo–16.44Co–2.45Nb–5.88W–Ni Balance, a directionally solidified (DS) superalloy IC10 (Alloy C) with the nominal composition of (0.07–0.12)C–(7.5–8.0)Cr–(11.5–12.5)Co–(4.7–5.2)W–(1.0–2.0)Mo–(6.5–7.5)Ta–(5.6–6.2)Al–(1.0–2.0)Hf–Ni Balance.

The mechanical properties for the three alloys at different temperatures, obtained from tension tests and fracture toughness tests, are listed in Table 1.

The servo-hydraulic testing system for FCPR tests was an MTS Landmark™ Model 370 load frame with a temperature controller and crack length measurement system, as shown in Fig. 1. All the tests were stress-controlled with cyclic frequency of 10–15 Hz and stress ratio $R=0.1$. FCPR tests were conducted with compact tension (CT) specimens with width $W=40$ mm and thickness $B=10$ mm. Crack length a was measured over the range of 8–30 mm, which corresponded to $a/W=0.2$–0.8. The test temperatures for the three superalloys were: 650 °C and 710 °C for Alloy A, 400 °C and 650 °C for Alloy B, and 650 °C for Alloy C, respectively. A slip-open furnace designed for CT specimens was the heating device. On one side of the furnace there was a small observing slot so that a direct recording of crack length might be possible by using a long focus microscope equipped with a digital camera. Because of high temperature interference, however, it was difficult to measure the crack length with the image acquisition system. Therefore the crack length measurement was made using the direct current potential drop (DCPD) method instead.

FCPR tests under constant maximum stress amplitude (CA) loading were carried out according to ASTM E647. Under this condition the stress intensity factors (SIF), K_{max}, K_{min} and $\Delta K=K_{max}-K_{min}$, were functions of crack length, a/W. The tests were controlled and the a–N data were recorded automatically by MTS software at crack increment of about $\Delta a=0.25$ mm for each specimen.

The overloading (OL) tests were basically the same as the CA tests. But during the tests, the single overload event with peak level of K_{OL} was applied manually. The overload ratio was defined by $R_{OL}=K_{OL}/K_{max}>1$, which is illustrated by the schematic drawing in Fig. 2. The applied overload ratios R_{OL} were 1.4 for Alloy A at 650 °C and 1.6 at 710 °C, 1.6 for Alloy B and 1.63 for Alloy C, respectively. In each specimen several overloading events were carried out. The crack growth increment between overloading events was about 3 mm.

Table 1
Mechanical properties and fracture toughness values of the three superalloys.

Alloys	Temperature [°C]	σ_b [MPa]	$\sigma_{0.2}$ [MPa]	K_C [MPa$\sqrt{m}$]
Alloy A	25	1,403	1,163	–
	650	1,150	976	98.8
	710	1,028	907	119.4
Alloy B	400	1,354	994	155.0
	650	1,306	985	137.9
Alloy C	25	910	666	90.0
	600	774	613	–
	700	757	634	–

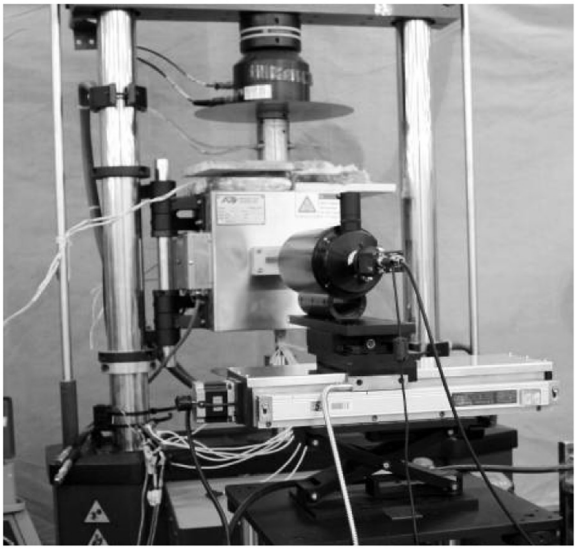

Fig. 1. Testing system for the presented FCPR experiments.

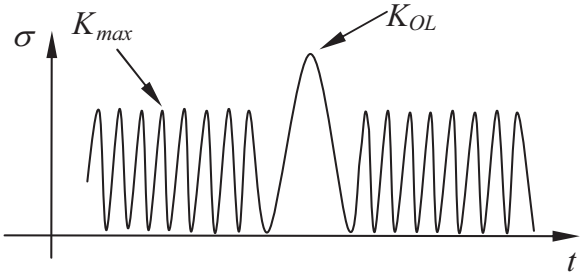

Fig. 2. Schematic drawing for illustrating the overloading event.

3. Results and discussions

3.1. *da/dN – ΔK data of CA fatigue tests*

The resulting plots of da/dN – ΔK of CA fatigue tests for Alloy A and Alloy B are shown in Fig. 3(a) and (b) respectively. For both of the superalloys, increasing FCPRs with increasing test temperature in the low ΔK range (<30 MPa$\sqrt{m}$) are evident. This is attributed to be high temperature induced oxidation at the crack tip [4]. But in the higher ΔK range (>40 MPa$\sqrt{m}$), the da/dN – ΔK curves of both materials at different temperatures are merged, which implies a temperature-independent behavior in the high ΔK range. But, in general, the difference between the two temperatures is not significant.

3.2. *Recorded a–N curves of CA fatigue tests with overloading*

The data of crack length a versus the number of cycles N (a–N curves) of each specimen were obtained for the three alloys. It is found that FCPR retardation after overloading occurred when the overload ratio is greater than or equal to 1.6 for the three alloys.

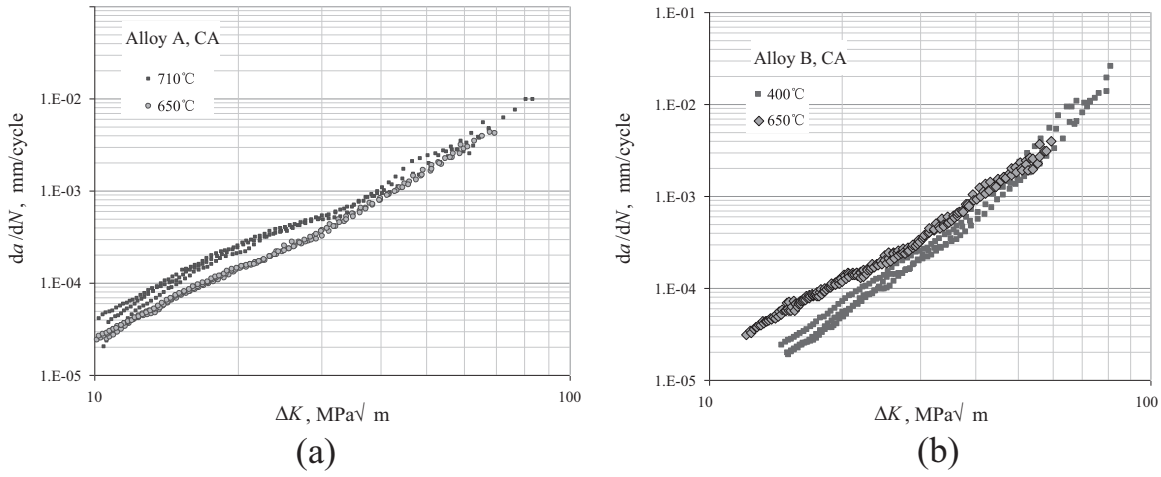

Fig. 3. FCPR data of CA fatigue tests (a) for Alloy A and (b) for Alloy B at high temperatures.

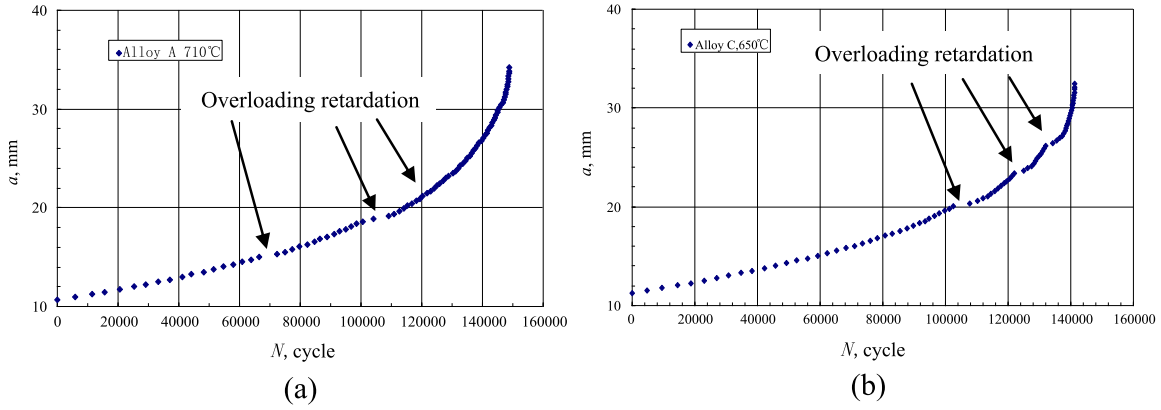

Fig. 4. Crack growth *a*–*N* curves (a) for Alloy A at 710 °C and (b) for Alloy C at 650 °C, showing crack growth retardation effect.

The results of Alloy A with overload ratio $R_{OL}=1.4$ at 650 °C, however, showed less retardation. Two typical *a*–*N* curves, Alloy A at 710 °C and Alloy C at 650 °C, as seen in Figs. 4(a) and (b) respectively, are chosen to show the overloading behavior. The retardation related cycles after overloading are on the order of tens of thousands, which is only a few percent of the whole fatigue life of the specimen. This implies that the crack growth retardation in these two materials is distinguishable but not very significant. This is also true for Alloy B.

3.3. *da/dN – ΔK data for overloading CA fatigue tests*

The d*a*/d*N* – Δ*K* data for tests with overloading were calculated by the secant method. For the three tested materials, the obtained d*a*/d*N* – Δ*K* data from each specimen cover a Δ*K* range of about 10 MPa$\sqrt{m}$ to 80 MPa$\sqrt{m}$.

The tests of Alloy A at 650 °C were conducted on two specimens. Four overloading events for each specimen with an overloading ratio $R_{OL}=1.4$ were applied. The obtained d*a*/d*N* – Δ*K* data from the two specimens, shown in Fig. 5(a), are marked by two different symbols. It is found that the FCPR overload retardation effect is almost not distinguishable. The tests of Alloy A at 710 °C were conducted with overload ratio $R_{OL}=1.6$. Three overloading events were applied. The d*a*/d*N* – Δ*K* data, shown in Fig. 5(b), however, show more significant FCPR overloading retardation effects than those in Fig. 5(a).

For the OL tests of Alloy B, two specimens were tested at temperature of 400 °C and one at 650 °C. Four or five overloading events with overload ratio $R_{OL}=1.6$ were applied to each specimen. The obtained d*a*/d*N* – Δ*K* data of the tests at 400 °C are shown in Fig. 5(c) and data of test at 650 °C are shown in Fig. 5(d). The data in Fig. 5(c), from two specimens at 400 °C, are marked by two different symbols. Although the data are showing large scatter, the FCPR overload retardation of the tests at both temperatures is significant.

For Alloy C with overloading at 650 °C, three overloading events with overload ratio $R_{OL}=1.63$ were applied. The d*a*/d*N* – Δ*K* data in Fig. 5(e) show significant FCPR overload retardation effect and, quite interestingly, the crack growth rate recovery process after overloads can be easily distinguished.

3.4. *Fractographic analysis*

The fracture surfaces of CT specimens of the three superalloys after OL tests were observed by a scanning electron microscope (SEM) QUANTA 600. The whole fracture surface of Alloy B specimen at 400 °C is shown in Fig. 6. Five dark lines on the surface, corresponding to the five overloading events, can be recognized although the lower two lines are not very clear. The numbers also indicate the associated overloading events. It can be observed that the whole crack surface looks quite flat, almost no shear lips can be found. The crack fronts marked by the five overloading lines appear not much curved, though the fifth line is more curved than the other four. This implies that the CT specimen width is thick enough and the stress state during crack propagation is more plane strain. It was found that the fracture surfaces for Alloy A and Alloy C specimens are similarly flat.

In order to understand the micro morphology of the fracture

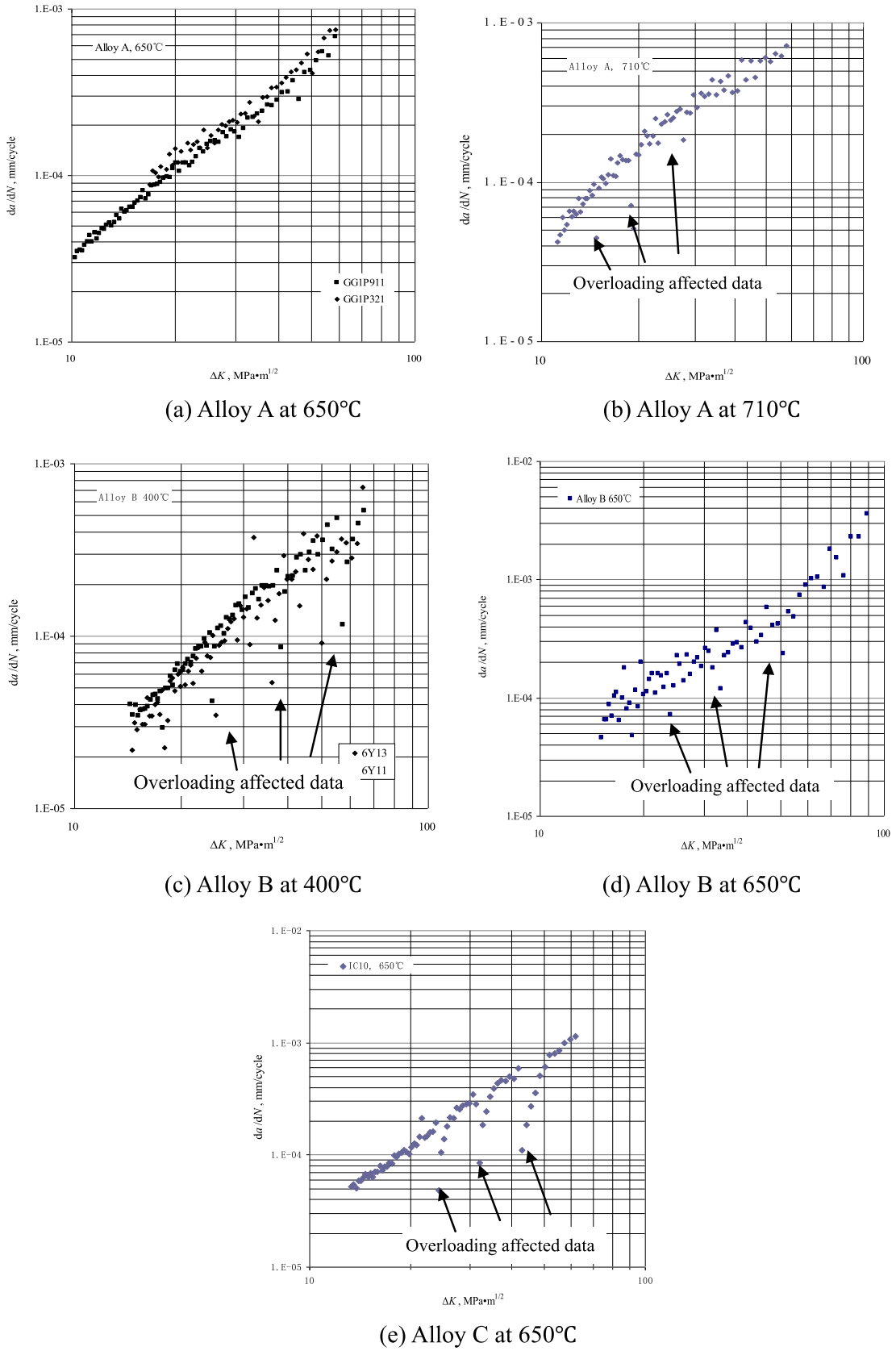

Fig. 5. FCPR da/dN – ΔK data for the three investigated superalloys. (a) Alloy A at 650 °C (b) Alloy A at 710 °C. (c) Alloy B at 400 °C (d) Alloy B at 650 °C. (e) Alloy C at 650 °C.

surfaces, some descriptions for overloading related areas on the fracture surfaces are introduced, as shown in Fig. 7. The crack surfaces are delineated as four parts: PART I, PART II, PART III and PART IV. PART I is the area from a point before overloading, A, to the position of the crack tip where overloading was applied, O. The crack length, A–O, is named as a_{before}. PART I is also named as the

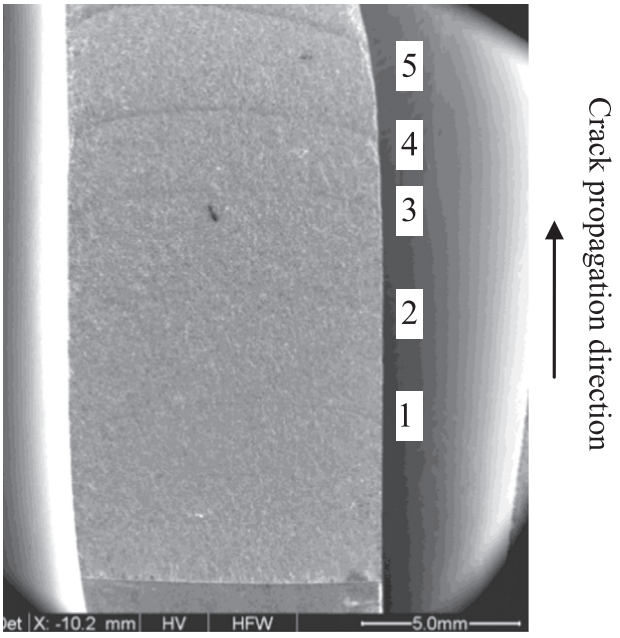

Fig. 6. Overall fracture surface of a specimen of Alloy B observed with SEM.

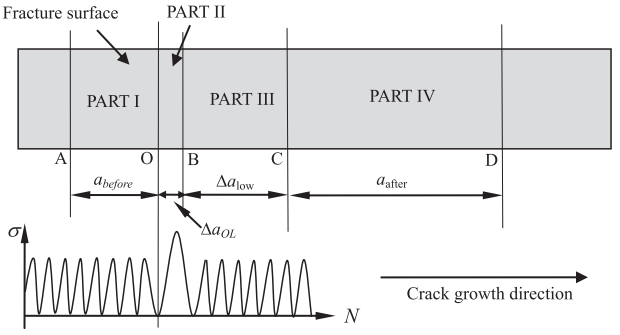

Fig. 7. Schematic illustration of overloading area near crack tip.

crack wake in view of the crack growth later on. During the overloading, there is a fast crack propagation induced by the large loading, Δa_{OL}, and this is the area identified as PART II from O to B. After overloading the crack retardation can happen if the overloading ratio is high enough. This area with low FCPR is called PART III, from B to C, is Δa_{low}. The FCPR will regain gradually to the normal rate from point C. The area from C to D is PART IV, and the length of this area is assumed a_{after}. The areas PART II and PART III are under the influence of overloading, while PART I and PART IV can be considered as normal FCPR areas.

The surface morphology of the specimen of Alloy A tested at 650 °C with overload ratio $R_{OL}=1.4$, the specimen of Alloy B tested at 400 °C with overload ratio $R_{OL}=1.6$ and the specimen of Alloy C tested at 650 °C with overload ratio $R_{OL}=1.63$, was investigated. SEM fractographs for the three materials, taken in the middle specimen area, are shown in Fig. 8(a), (b) and (c) respectively. The arrows beside Fig. 8 indicate the fatigue crack propagation direction.

The four part areas on the specimen surface of Alloy A are outlined by three solid lines, as shown in Fig. 8(a). The letters at right-hand side indicate the position of overloading (O), retardation start point (B) and finish point (C). These points are corresponding to the same letters in Fig. 7. In PART I, the regular fatigue striations, characterizing transgranular crack propagation, are evident. Meanwhile obvious abrasion was observed, which indicates crack surface friction near the overloading area, PART II. It

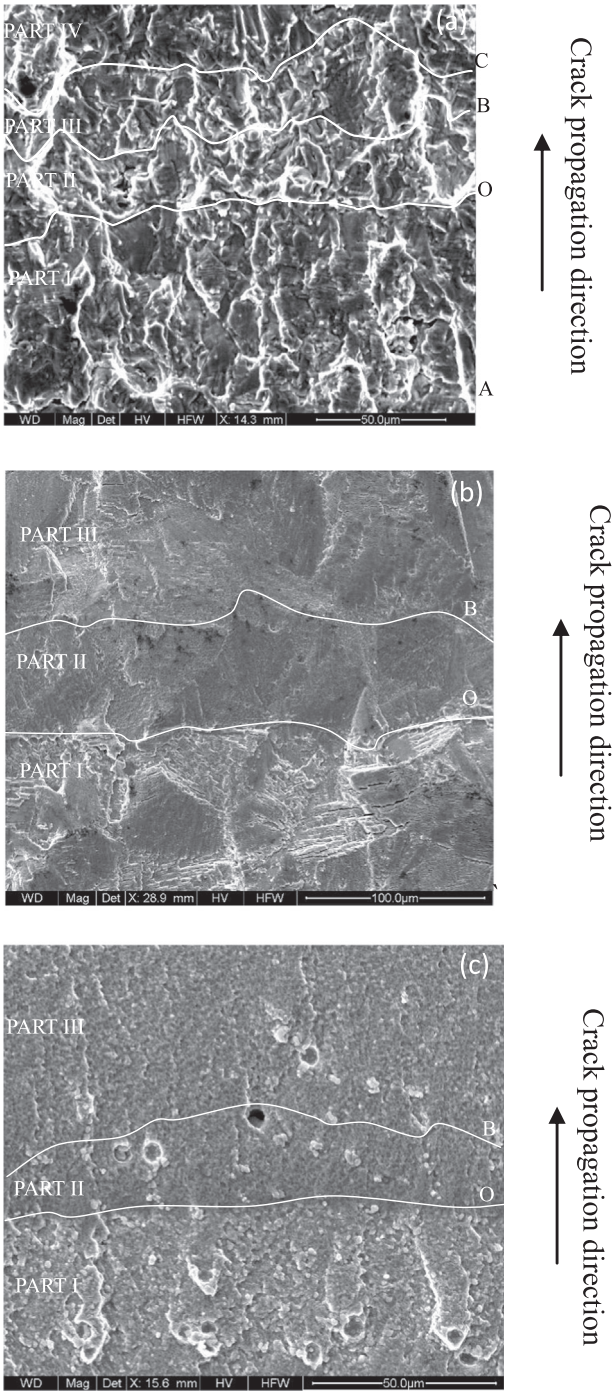

Fig. 8. Fractography of the specimens' surface near overload area: (a)Alloy A at 650 °C, (b)Alloy B at 400 °C, (c) Alloy C at 650 °C.

should be noted that near the line at position O, a hump induced by overloading seems quite high, and is accompanied with some secondary cracks. This is the trace of another crack path in a different direction, which stopped propagating for some reason. In PART III, it is hard to find fatigue striations because of the lower FCPR in this area. In PART IV, then, the fatigue striations become more distinguishable although the width of striations is not as large as that before overloading in PART I. It is considered that the FCPR regains its normal state.

The fracture surface of Alloy B tested at 400 °C with overload ratio $R_{OL}=1.6$ is shown in Fig. 8(b). The fatigue striations can be recognized easily and transgranular crack propagation is evident.

But the feature of crack surface contact is also significant since most striations are to some extent flattened. The four areas on the crack surface are distinguishable. For example, in PART II, almost no striations can be found. But in PART III, very fine striation-like patterns can be found because of the low FCPR.

The fracture surface of Alloy C tested at 650 °C with overload ratio $R_{OL}=1.63$ is shown in Fig. 8(c). In contrast to the other alloys shown in Fig. 8(a) and (b), it shows very significant crack surface contact, and almost all crack striations were erased. Although it is hard to distinguish the four areas, we suggest one outline shown in Fig. 8(c) and try to analyze the overloading influence. It is found that, while the length of overloading area PART II, Δa_{OL}, is short, the length of the low FCPR area PART III, Δa_{low}, is much longer compared with the ones of the other two alloys.

3.5. Mechanism of FCPR retardation after overloading

There are several mechanisms to explain FCPR retardation after overloading in OL tests. It is believed that retardation may be attributed to two main reasons in the present discussion. One is the plastic zone mechanism, and another is the crack wake mechanism. Both of these belong to the crack closure theory, which are believed applicable to the studied materials.

3.5.1. Plastic zone in front of crack tip

Since the overload effect is related to the local stress state near the crack tip the study was focused on the crack tip plastic zone induced by CA loading and overloading OL. And a schematic illustration of plastic zone in front of crack tip is shown in Fig. 9. The rectangular frame is a representation of part of the crack tip region on a free surface of a CT specimen. The local stress distribution in the direction perpendicular to the crack surface in the front area of crack tip along x axis, $\sigma_y(x)$, is not constant. Near the crack tip, the stress is at the ultimate strength level and then decreases rapidly. The overload stress curve $\sigma_y(x)_{OL}$ is shown in Fig. 9. This assumption is based on the stress-strain responses of the materials being of the elasto-plastic type. This is true for most ductile alloys, and it holds also for the superalloys in the present study. The area in which the stress level is above the elastic limit is the plastic zone. The shape of the plastic zone in front of the crack tip is assumed to be an ellipse with its long axis in x direction. In Fig. 9, the plastic zone created by the single overloading, SOPZ, is described as a gray ellipse and its diameter along x is r_{OL}; the plastic zone created by CA loading, CPZ (cyclic plastic zone), is an ellipse in black, and its diameter is r_p. The size of the plastic zone depends on the applied loading. The higher the loading, the larger the resulting plastic zone will be. Since the overload ratio $R_{OL}=1.6$ is greater than 1, it is possible that the r_{OL} is much larger than the r_p. Similar to the definitions in Fig. 7, the crack length before overloading is a, the crack increment induced by the overloading event is Δa_{OL} and the propagating length with the low FCPR denoted as Δa_{low}.

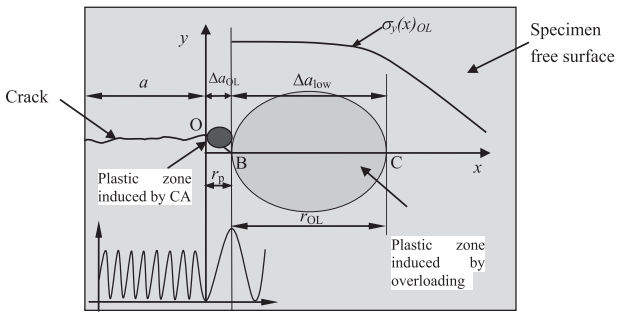

Fig. 9. A schematic illustration of plastic zone in front of crack tip.

The plastic zone is understood as the concept of residual stress. If we take a view of material damage, some different ideas can be obtained. It is well-known that fatigue damage is a kind of irreversible dislocation stack-up along slip bands. Let us imagine that, if the fatigue damage in the CPZ (the black elliptical area in Fig. 9) is accumulated through many cycles, e.g. 10^4 cycles, the material damage must be quite severe in CPZ area. During the overloading event, the crack progresses a large step and must be over the CPZ size, i.e. $\Delta a_{OL} \geq r_p$. At the same time a large SOPZ is induced (the gray elliptic area in Fig. 9), which is a non-fatigue damaged zone. Consequently, it takes cycles to rebuild a new CPZ in the SOPZ. Moreover, due to the compressive residual stress in the SOPZ, it needs more cycles than before overloading to rebuild the CPZ. These all make the FCPR decreasing dramatically. But once the new CPZ, i.e. fatigue damaged zone, is created the crack will start to grow again. With a decrease of the residual compressive stress the FCPR will speed-up gradually, and eventually regain its rate before overloading. Therefore the size of SOPZ, r_{OL}, is almost the size of low FCPR region, Δa_{low}. This mechanism is supported by the fractographic observation, as mentioned above.

The FCPR retardation mechanism analyzed above is in a quite ideal condition. In fact, there are many "exceptional" situations. For example, if the overloading induces a large crack with a sharp tip, the FCPR may not decrease very much. The test of alloy A at 650 °C exhibits this case. It can be found from Fig. 8(a) that a crack is along the line of point O, this indicates a sharp crack tip induced by overload. This is one reason why the overload retardation of alloy A at 650 °C is not significant, as shown in Fig. 5(a). Another reason may be attributed to the low overload ratio as the induced SOPZ is also small and the residual compressive stress inside is low.

Under the test condition at high temperatures, the stress relief is possible, whatever the overloading ratio R_{OL} is, larger or less than 1.0. For the present study, the residual stress in SOPZ is also relieved to some extent. Consequently, the retardation effect is not very significant compared to the effects of tests at room temperature.

3.5.2. Mechanism based on crack wake contact

Another mechanism which may play a role in the FCPR retardation effect is deformation in the crack wake. This mechanism considers the effects of the large plastic deformation induced by overloading in PART I and PART II. In fact, the crack propagation induced deformation in the crack wake is a normal phenomenon. Here the deformation induced by the constant amplitude loading is referred as CA crack wake, while the ridge produced by the large overloading (overload ratio $R_{OL} > 1.0$) is referred as OL crack wake, which is much higher than the CA crack wake. The higher OL crack wake hinders the crack face contact. Therefore the crack growth driving force is reduced, which is represented by an effective stress intensity factor ΔK_{eff}. Consequently, the ΔK_{eff} after overloading is lower than the ΔK_{eff} before overloading and the FCPR decreases. This is one reason for crack retardation after overloading.

In addition, the blunt crack tip induced by overloading can also be a barrier because it takes time to rebuild a sharp crack tip.

4. Conclusions

From the CA fatigue experimental results of the three superalloys it was found that, for superalloys Alloy A and Alloy B, increasing FCPRs with test temperature in the low ΔK range ($< 30\ \mathrm{MPa}\sqrt{\mathrm{m}}$) are evident. But in the higher ΔK regime, the temperature-induced FCPR increase vanishes.

According to the experimental data of fatigue tests with single overload, it is found that the FCPRs of the investigated materials

were retarded after overloading events with overload ratio $R_{OL}=1.6$ for all the three alloys. The possible mechanism of overload retardation effect is related to crack closure. Two aspects of crack closure, the plastic zone and the deformation in crack wake, are discussed. The size of the plastic zone in front of the crack tip is proportional to the loading or overloading levels, based on the theory of material mechanics. And, perhaps more importantly, the fatigue damage in the cyclic plastic zone can be a more influential factor on overload retardation. At the same time, the deformation in the crack wake also play a role in overloading behavior.

References

[1] J.M. Larsen, T. Nicholas, Eng. Fract. Mech. 22 (4) (1985) 713–730.
[2] M. Clavel, A. Pineau, Mater. Sci. Eng. 55 (1982) 157–171.
[3] Y.L. Lu, P.K. Liaw, G.Y. Wang, M.L. Benson, S.A. Thompson, J.W. Blust, et al., Mater. Sci. Eng. A 397 (2005) 122–131.
[4] D.E. Macha, Eng. Fract. Mech. 12 (1) (1979) 1–11.
[5] A. Defresne, L. Remy, Mater. Sci. Eng. A129 (1990) 55–64.
[6] C. Mercer, A.B.O. Soboyejo, W.O. Soboyejo, Mater. Sci. Eng. A270 (1999) 308–322.
[7] M.A. Hicks, J.E. King, Int. J. Fatigue 5 (2) (1983) 67–74.
[8] J. Schijve, Fatigue of Structures and Materials, Springer Science+Business, Germany, 2009.
[9] S. Pommier, Int. J. Fatigue 25 (2003) 983–997.
[10] S.Y. Lee, P.K. Liaw, H. Choo, R.B. Rogge, Acta Mater. 59 (2) (2011) 485–494.
[11] R. Pippan, K. Haberz, H.P. Stüwe, Eng. Fract. Mech. 53 (3) (1996) 441–448.
[12] A. Pineau, S.D. Antolovich, Eng. Failure Anal. 16 (2009) 2668–2697.
[13] B. Lawless, S.D. Antolovich, C. Bathias, B. Boursier, Fracture: Interactions of Microstructure, Mechanisms and Mechanics, TMS-AIME, Warrendale, PA 1985, pp. 285–301.